

Hydroxychloroquine in the treatment and prophylaxis of SARS-CoV-2 infection in non- human primates

CURRENT STATUS: UNDER REVIEW

natureresearch

Pauline Maisonnasse

Université Paris-Saclay, Inserm, CEA, Center for Immunology of Viral, Auto-immune, Hematological and Bacterial diseases » (IMVA-HB/IDMIT), Fontenay-aux-Roses & Le Kremlin-Bicêtre, France

Jérémie Guedj

Université de Paris, INSERM, IAME, F-75018 Paris, France

Vanessa Contreras

Université Paris-Saclay, Inserm, CEA, Center for Immunology of Viral, Auto-immune, Hematological and Bacterial diseases » (IMVA-HB/IDMIT), Fontenay-aux-Roses & Le Kremlin-Bicêtre, France

Sylvie Behillil

Unité de Génétique Moléculaire des Virus à ARN, GMVR : Institut Pasteur, UMR CNRS 3569, Université de Paris, Paris, France. Centre National de Référence des Virus des infections respiratoires (dont la grippe), Institut Pasteur, Paris, France.

Caroline Solas

Aix-Marseille Univ, APHM, Unité des Virus Emergents (UVE) IRD 190, INSERM 1207, Laboratoire de Pharmacocinétique et Toxicologie, Hôpital La Timone, 13005 Marseille, France

Romain Marlin

Université Paris-Saclay, Inserm, CEA, Center for Immunology of Viral, Auto-immune, Hematological and Bacterial diseases » (IMVA-HB/IDMIT), Fontenay-aux-Roses & Le Kremlin-Bicêtre, France

Thibaut Naninck

Université Paris-Saclay, Inserm, CEA, Center for Immunology of Viral, Auto-immune, Hematological and Bacterial diseases » (IMVA-HB/IDMIT), Fontenay-aux-Roses & Le Kremlin-Bicêtre, France

Andres Pizzorno

CIRI, Centre International de Recherche en Infectiologie, (Team VirPath), Univ Lyon, Inserm, U1111, Université Claude Bernard Lyon 1, CNRS, UMR5308, ENS de Lyon, F-69007, Lyon, France

Julien Lemaitre

Université Paris-Saclay, Inserm, CEA, Center for Immunology of Viral, Auto-immune, Hematological and Bacterial diseases » (IMVA-HB/IDMIT), Fontenay-aux-Roses & Le Kremlin-Bicêtre, France

Antonio Gonçalves

Université de Paris, INSERM, IAME, F-75018 Paris, France

Nidhal Kahlaoui

Université Paris-Saclay, Inserm, CEA, Center for Immunology of Viral, Auto-immune, Hematological and Bacterial diseases » (IMVA-HB/IDMIT), Fontenay-aux-Roses & Le Kremlin-Bicêtre, France

Olivier Terrier

CIRI, Centre International de Recherche en Infectiologie, (Team VirPath), Univ Lyon, Inserm, U1111, Université Claude Bernard Lyon 1, CNRS, UMR5308, ENS de Lyon, F-69007, Lyon, France

Raphael Ho Tsong Fan

Université Paris-Saclay, Inserm, CEA, Center for Immunology of Viral, Auto-immune, Hematological and Bacterial diseases » (IMVA-HB/IDMIT), Fontenay-aux-Roses & Le Kremlin-Bicêtre, France

Vincent Enouf

Unité de Génétique Moléculaire des Virus à ARN, GMVR : Institut Pasteur, UMR CNRS 3569, Université de Paris, Paris, France. Centre National de Référence des Virus des infections respiratoires (dont la grippe), Institut Pasteur, Paris, France. Plate-forme de microbiologie mutualisée (P2M), Pasteur International Bioresources Network (PIBnet), Institut Pasteur

Nathalie Dereuddre- Bosquet

Université Paris-Saclay, Inserm, CEA, Center for Immunology of Viral, Auto-immune, Hematological and Bacterial diseases » (IMVA-HB/IDMIT), Fontenay-aux-Roses & Le Kremlin-Bicêtre, France

Angela Brisebarre

Unité de Génétique Moléculaire des Virus à ARN, GMVR : Institut Pasteur, UMR CNRS 3569, Université de Paris, Paris, France. Centre National de Référence des Virus des infections respiratoires (dont la grippe), Institut Pasteur, Paris, France.

Franck Toure

Unité des Virus Emergents, UVE: Aix Marseille Univ, IRD 190, INSERM 1207, IHU Méditerranée Infection, 13005, Marseille, France.

Catherine Chapon

Université Paris-Saclay, Inserm, CEA, Center for Immunology of Viral, Auto-immune, Hematological and Bacterial diseases » (IMVA-HB/IDMIT), Fontenay-aux-Roses & Le Kremlin-Bicêtre, France

Bruno Hoen

Emerging Diseases Epidemiology Unit, Institut Pasteur, Paris, France

Bruno Lina

CIRI, Centre International de Recherche en Infectiologie, (Team VirPath), Univ Lyon, Inserm, U1111, Université Claude Bernard Lyon 1, CNRS, UMR5308, ENS de Lyon, F-69007, Lyon, France; Laboratoire de Virologie, Centre National de Référence des Virus des infections respiratoires (dont

la grippe), Institut des Agents Infectieux, Groupement Hospitalier Nord, Hospices Civils de Lyon, 69004 Lyon, France

Manuel Rosa Calatrava

CIRI, Centre International de Recherche en Infectiologie, (Team VirPath), Univ Lyon, Inserm, U1111, Université Claude Bernard Lyon 1, CNRS, UMR5308, ENS de Lyon, F-69007, Lyon, France

Sylvie van der Werf

Unité de Génétique Moléculaire des Virus à ARN, GMVR : Institut Pasteur, UMR CNRS 3569, Université de Paris, Paris, France. Centre National de Référence des Virus des infections respiratoires (dont la grippe), Institut Pasteur, Paris, France.

Xavier de Lamballerie

Unité des Virus Emergents, UVE: Aix Marseille Univ, IRD 190, INSERM 1207, IHU Méditerranée Infection, 13005, Marseille, France.

Roger Le Grand

Université Paris-Saclay, Inserm, CEA, Center for Immunology of Viral, Auto-immune, Hematological and Bacterial diseases » (IMVA-HB/IDMIT), Fontenay-aux-Roses & Le Kremlin-Bicêtre, France

10.21203/rs.3.rs-27223/v1

SUBJECT AREAS

Virology

KEYWORDS

SARS-CoV-2, macaques, hydroxychloroquine, azithromycin, viral load levels

Abstract

COVID-19 has become a pandemic that has caused over 200,000 deaths worldwide, with no antiviral drug or vaccine yet available. Several clinical studies are ongoing to evaluate the efficacy of repurposed drugs that have demonstrated antiviral efficacy *in vitro*. Among these candidates, hydroxychloroquine (HCQ) has been given to thousands of individuals worldwide but definitive evidence for HCQ efficacy in treatment of COVID-19 is still missing.

We evaluated the antiviral activity of HCQ both *in vitro* and in SARS-CoV-2-infected macaques. HCQ showed antiviral activity in monkey African green monkey kidney (VeroE6) cells but not in a model of reconstituted human airway epithelium. In macaques, we tested different treatment strategies in comparison to placebo, before and after peak viral load, alone or in combination with azithromycin (AZTH). Neither HCQ nor HCQ+AZTH showed a significant effect on the viral load levels in any of the tested compartments. When the drug was used as a pre-exposure prophylaxis (PrEP), HCQ did not confer protection against acquisition of infection.

Our findings do not support the use of HCQ, either alone or in combination with AZTH, as an antiviral treatment for COVID-19 in humans.

Main Text

The emergence of severe acute respiratory syndrome coronavirus 2 (SARS-CoV-2), which is the causative agent for COVID-19 and originated in Wuhan, China, in 2019, has developed quickly into a global pandemic that has already caused over 200,000 deaths worldwide. COVID-19 is characterized by initial mild disease associated with respiratory symptoms at the peak of viral replication 1. Nasal and tracheal peaks of viral load occur close to the time of mild symptom onset, and viral load declines afterwards 2. In some patients, a late severe immunological syndrome occurs 6 to 14 days after onset of symptoms, characterized by high levels of inflammatory proteins (a “cytokine storm”) 3. This may require intensive care and is responsible for most of the fatalities 2,4,5. Since no cure or prophylaxis is yet available against COVID-19, the World Health Organization (WHO) has provided recommendations for using investigational anti-COVID therapeutics in approved, randomized, controlled clinical trials or, if not possible, under Monitored Emergency Use of Unregistered

Interventions Framework (MEURI, WHO/2019-nCoV/clinical/2020.4).

Hydroxychloroquine sulfate (HCQ) has well documented *in vitro* activity against various viruses 6 and has emerged as an active compound against SARS-CoV-2 from different screening programs, including a 1,520 library of FDA-approved compounds 7. In VeroE6 cells, HCQ has a 50% maximal effective concentration (EC50) varying between 0.7 and 4 μM , as recently reported 7-9. HCQ may inhibit viral transport in endosomes by alkalinizing the intra-organelle compartment 9,10. In addition, it was suggested that chloroquine and its derivatives might interfere with glycosylation mechanisms, as reported for other viruses 11, and this activity on the angiotensin convertase enzyme 2 (ACE2) and the virus spike protein may potentially affect infectivity. Moreover, the drug may also act as an immunomodulatory agent 12,13. In lupus, HCQ decreases the level of inflammatory cytokines such as IL-1 β , IL-6 and TNF- α 10,14,15, which may be relevant for COVID-19 3. Furthermore, it has been proposed that azithromycin (AZTH), which displays *in vitro* antiviral activity against SARS-COV-2 7,16, could potentiate the efficacy of HCQ¹⁷.

Based on these properties, HCQ has been considered for COVID-19 treatment, alone or in combination with AZTH, but the results of clinical studies are still inconclusive 17,18 or pending.

Based on previous studies of SARS-COV and MERS-COV infection, we and others have set up experimental models of non-human primates (NHP) infected with SARS-CoV-2 that reproduce human infection and make possible the evaluation of drug efficacy in well-controlled settings 19,20. Here we used our model of cynomolgus macaque (*Macaca fascicularis*) to test different treatment strategies with HCQ, alone or in combination with AZTH, before or after the peak of viral replication. We also tested HCQ administration as pre-exposure prophylaxis (PrEP) against SARS-CoV-2 infection.

In vitro efficacy of hydroxychloroquine against SARS-CoV-2 infection

We first evaluated the *in vitro* antiviral activity of HCQ against a SARS-CoV-2 virus isolated from one of the first COVID-19 patients in France. Post-infection treatment of Vero E6 cells with HCQ resulted in a dose-dependent antiviral effect, with 50% inhibitory concentration (IC50) values of 2.2 μM (0.7 $\mu\text{g}/\text{mL}$) and 4.4 μM (1.4 $\mu\text{g}/\text{mL}$) at 48 and 72 hours pi, respectively, which is in the range of 0.7 to 4 μM previously published 21 (Extended Data Fig. 1a). We next studied infection in the reconstituted

human airway epithelium MucilAir™ model (HAE) developed from primary nasal or bronchial cells differentiated and cultivated in the air/liquid interphase 22. Unlike our previous observations for remdesivir 23, the antiviral activity of HCQ in Vero E6 cells did not translate to the HAE, with doses of 1 μ M or 10 μ M failing to reduce significantly SARS-CoV-2 apical viral titers at 48 hpi (Extended Data Fig. 1b). HCQ also did not protect the epithelial integrity during infection, as evidenced by trans-epithelial electrical resistance (TEER) values comparable to untreated cells and significantly lower than those of the mock-infected controls.

Infection of macaques with SARS-CoV-2

Cynomolgus macaques were infected on day 0 with a total dose of 10⁶ pfu of a primary SARS-CoV-2 isolate (BetaCoV/France/IDF/0372/2020) (passaged twice in VeroE6 cells) by combined intra-nasal and intra-tracheal routes. Control animals (CTRL, n=8) had high viral load levels in nasopharyngeal and tracheal samples (swabs), as estimated by RT-qPCR, as early as day 1 post infection (1 dpi). In tracheal samples, the viral load peaked at 2 dpi (Fig. 1b, Extended Data Fig. 2a), with a median (min-max) peak value of 7.9log₁₀ copies/mL. Afterward, viral loads progressively decreased and most animals had undetectable viral load by 10 dpi. Similar profiles were observed for nasal shedding (Extended Data Fig. 2b), whereas low viral loads were detected for more than 3 weeks in rectal samples and broncho-alveolar lavages (Extended Data Fig. 2c,d). Animals exhibited mild clinical signs, as reported in the majority of human cases during the early infection period, including early lymphopenia (2 dpi) and coughing or sneezing without dyspnea (Extended Data Fig. 5). No major changes were observed regarding heart rate, respiratory rate, and oximetry. Interestingly, typical focal ground glass opacities associated with pleural thickening 24,25 were observed by CT scan with variable degrees of severity (Fig. 2, Extended Data Fig. 3). Lesions were detectable as early as 2 dpi and persisted up to 13 dpi in some animals. None of the control animals developed an immunological syndrome similar to what is observed in the late stages of the severe forms of the human disease.

Treatment with hydroxychloroquine

To assess the anti-viral efficacy of HCQ, macaques received HCQ daily by gavage for ten days or more. A dosing regimen of 90 mg/kg on day 1 pi (loading dose) followed by a daily maintenance dose

of 45 mg/kg was identified in a group of uninfected animals as capable of generating clinically relevant drug exposure (Extended Data Fig. 4b). In parallel, we also tested a lower dosing regimen, with a loading dose of 30 mg/kg and a maintenance dose of 15 mg/kg. Overall, 9 animals were infected at day 0 and treated at 1 dpi using the high dosing regimen (Hi D1, n=5) or the low dosing regimen (Lo D1, n=4). We also examined the effect of a late treatment starting at 5 dpi, when viral loads are 3 to 4 logs lower as compared with peak values, to evaluate the benefit of HCQ in accelerating the virus clearance (Lo D5, n=4).

All treated animals had tracheal viral load kinetics similar to those of untreated animals, with median peak viral load of 7.1 and 7.5 log₁₀ copies/mL in Hi D1 and Lo D1, respectively, compared with 7.9 log₁₀ copies/mL in the CTRL group. Likewise, the areas under the curve (AUC) of viral load were similar, with values of 36.9 and 39.7 log₁₀ copies.day/mL, as compared with 40.3 log₁₀ copies.day/mL in CTRL animals (p=0.62 and 0.37, respectively). Similar results were obtained in nasal swabs, and there were no differences in the levels of viral replication in broncho-alveolar lavages (Fig. 1d, Extended Data Fig. 2). In animals treated from 1 dpi or 5 dpi, HCQ did not accelerate the time to viral clearance, and the median times to first unquantifiable viral load were 4.5, 7.0, 7.0, and 7.0 days in the CTRL, Lo D1, Hi D1, and Lo D5 groups, respectively.

Next we evaluated the (HCQ + AZTH) combination therapy administered from day 1 pi (Hi D1 + AZTH, n=5), with AZTH given at a loading dose of 36 mg/kg followed by a daily dose of 18 mg/kg to mimic human exposure. No impact of treatment was observed on either viral load in the different compartments or clinical scores. Clinical signs were comparable to controls, with some animals exhibiting high CT scores in the Hi D1 + AZTH group (Fig 2). In parallel, we also treated animals with a high dose of HCQ, starting 7 days before viral challenge as pre-exposure prophylaxis (PrEP, n=5). Again, the kinetics of viral loads were similar to those of the control group with no reduction in terms of AUC, peak viral load or time to first unquantifiable viral load (Fig. 1, Extended Data Fig. 2).

Relation between HCQ concentration levels and viral kinetics

In the animals of Hi D1, Hi D1+AZTH and PrEP groups, the plasma exposures were comparable to those observed in routine clinical practice 3-5 days after HCQ initiation using a 200 mg three times

daily dose (C Solas, data from the Pharmacokinetics and Toxicology Laboratory) (Fig. 3a). Drug trough concentrations were lower in both the Lo D1 and Lo D5 groups. When we assessed whether the higher drug exposure could generate more rapid virus clearance, neither the time to attain the viral load limit of quantification, nor the peak viral load were significantly associated with plasma HCQ concentrations (Fig. 3b-d). Finally, in an additional group of uninfected macaques, we characterized the HCQ pharmacokinetic profile in blood and plasma as the drug accumulation in lung 6 days after treatment initiation (Fig. 3e-f, Extended Data Fig. 4). The blood concentrations in Hi HCQ were higher than 1.4 µg/mL, showing that the drug concentrations in blood remained above the drug EC50 identified in VeroE6 cells during the dosing period (see above). Drug concentrations were even higher in lung tissues with a lung to plasma ratio ranging from 27 to 177 (Fig. 3f), allowing lung tissues to achieve concentrations above the drug EC50 in VeroE6 cells in all animals during the dosing period.

Immunopathogenesis and host response to hydroxychloroquine treatment

High alanine aminotransferase (ALAT) and creatinine kinase levels were observed in animals treated with the high HCQ and particularly the HCQ+AZTH regimen compared with controls (Extended Data Fig. 7 and 8). The signs of liver toxicity observed in macaques exposed to high HCQ doses of high HCQ +AZTH doses would limit the use of increased doses of HCQ for the treatment of COVID-19 in humans.

HCQ treatment did not prevent lymphopenia (Extended Data Fig. 5) nor pulmonary lesions, as evidenced by CT (Fig. 2, Extended Data Fig. 3). Similar lesion scores were observed in controls and treated animals.

All animals exhibited an increase of type I IFN- α , IL-1RA, CCL2 and CCL11 in plasma at day 2 pi (Fig. 4, Extended Data Fig. 6). In addition, IL-15 peaked early during infection, suggesting a role for innate lymphoid cells in the control of initial viral replication in both treated and untreated animals.

Interestingly, when compared with controls, TNF- α was significantly increased and IL-1RA was significantly reduced at day 2 pi (Fig. 4, Extended Data Fig. 6) in the groups that received the high dose of HCQ alone ($p=0.032$ and $p=0.028$, respectively) or with AZTH ($p=0.037$ and $p=0.045$, respectively). This may reflect the immunomodulatory properties of these drugs.

Conclusions

Our study establishes that SARS-CoV-2 infection in cynomolgus macaques provides a relevant model for studying the early stages of COVID infection in humans and is appropriate for the preclinical evaluation of antiviral candidate molecules 2,4,5,26,19,20. Our experiments showed no antiviral activity nor clinical efficacy of HCQ treatment, regardless of the timing of treatment initiation, either before infection, early after infection (before viral load peak) or late after infection (after viral load peak). This was in spite of high drug concentration in blood and lung and plasma exposure similar to that observed in COVID patients treated with HCQ. Thus, treatment with HCQ is unlikely to have antiviral activity in respiratory compartments in humans. Our results illustrate the frequent discrepancy between results from *in vitro* classic assays and *in vivo* experiments, as reported for other viral infections such as influenza, dengue or chikungunya, where clinical trials failed to demonstrate efficacy of chloroquine or HCQ 6,27.

In conclusion, our results evaluation of HCQ in a non-human primate model of COVID-19 does not support its use as an antiviral agent for the treatment of COVID-19 in humans.

Methods

Ethics and biosafety statement

Cynomolgus macaques (*Macaca fascicularis*), aged 37-40 months and originating from Mauritian AAALAC certified breeding centers were used in this study. All animals were housed in IDMIT infrastructure facilities (CEA, Fontenay-aux-roses), under BSL-2 and BSL-3 containment when necessary (Animal facility authorization #D92-032-02, Prefecture des Hauts de Seine, France) and in compliance with European Directive 2010/63/EU, the French regulations and the Standards for Human Care and Use of Laboratory Animals, of the Office for Laboratory Animal Welfare (OLAW, assurance number #A5826-01, US). The protocols were approved by the institutional ethical committee "Comité d'Ethique en Expérimentation Animale du Commissariat à l'Énergie Atomique et aux Énergies Alternatives" (CEtEA #44) under statement number A20-011. The study was authorized by the "Research, Innovation and Education Ministry" under registration number APAFIS#24434-2020030216532863v1.

Hydroxychloroquine and azithromycin

Hydroxychloroquine sulfate was manufactured for Sanofi by the Chinoin Pharmaceutical and Chemical works (Budapest, Hungary) under Good Manufacturing Practice (GMP) conditions and provided as the base powder. Batch number DU017 was solubilized extemporaneously in water at 5, 10 or 15 mg/mL depending on the group and the dose. Azithromycin 250 mg tablets (Sandoz, France; batch number KH5525) were crushed and suspended extemporaneously at 12 mg of AZTH per mL in water.

Animals and study design

To evaluate the efficacy of HCQ and HCQ+AZTH treatments, the animals were randomly assigned in sex balanced experimental groups. Challenged animals were exposed to a total dose of 10⁶ pfu of SARS- CoV-2 *via* the combination of intranasal and intra-tracheal routes (Day 0), using atropine (0.04 mg/kg) for pre-medication and ketamine (5mg/kg) with medetomidine (0.042 mg/kg) for anesthesia. The “high dose” regimen in group “Hi D1” (n=5) consisted of a loading dose of 90 mg/kg at 1 dpi and a daily maintenance dose of 45 mg/kg, for a total of 10 days. The “Hi D1+AZTH” group (n=5) regimen consisted of the same HCQ regimen as for the Hi D1 group combined with one loading dose of 36 mg/kg of AZTH at 1 dpi, followed by a daily maintenance dose of 18 mg/kg AZTH, for 10 days. The “low dose” (Lo) regimen consisted of a HCQ loading dose of 30 mg/kg and a daily maintenance dose of 15 mg/kg for 12 days. The low dose treatment of the “Lo D1” group (n=4) was initiated at day 1 pi and the low dose treatment of the “Lo D5” group (n=4) was initiated at 5 dpi. The PrEP group (n=5) regimen consisted of a loading dose of 30 mg/kg seven days before challenge, followed by a daily dose of 15 mg/kg for four days and the 45 mg/kg for three days before virus challenge, and then until day 6 pi. Treatments were delivered by gavage. Placebo animals received water, which was the vehicle for HCQ. Animals were observed daily and clinical exams were performed at baseline, daily for one week, and then twice weekly, on anaesthetized animals using ketamine (5 mg/kg) and medetomidine (0.042 mg/kg). Body weight, rectal temperature, respiration, heart rates and oxygen saturation were recorded and blood, as well as nasal, tracheal and rectal swabs, were collected. Broncho-alveolar lavages (BAL) were performed using 30 mL sterile saline on 6, 14, 21 and 28 dpi. Chest CT was performed at baseline and on 2, 5 and 11/13 dpi in anesthetized animals using tiletamine (4 mg/kg) and zolazepam (4 mg/kg). Blood cell counts, haemoglobin and haematocrit were

determined from EDTA blood using a HMX A/L analyzer (Beckman Coulter). Biochemistry parameters (ALAT, ASAT, albumin, haptoglobin, creatinine, creatine kinase, LDH and total protein) were analyzed with standard kits (Siemens) and C- reactive protein with a canine kit (Randox) in lithium heparin plasma, inactivated with Triton X-100, using ADVIA1800 analyzer (Siemens).

The pharmacokinetics of HCQ was assessed using the same administration procedure in 6 uninfected animals, randomly assigned by pairs in 3 experimental groups as described in **Extended Data Fig. 4**. The “PK Lo” group received a low loading dose (30 mg/kg) at day 0 and a low daily maintenance dose (15 mg/kg) for 5 days. The “PK Hi” and “PK Hi + AZTH” groups received a high loading HCQ dose (90 mg/kg) on day 0 and a high daily maintenance dose (45 mg/kg) for 6 days, along with AZTH for the second group (loading dose of 36 mg/kg and maintenance of 18 mg/kg). Blood samples were taken at 0, 2, 4, 6 hours post-treatment (hpt) on day 0, and before treatment on the following days. For the “PK Hi” and “PK Hi + AZTH” groups, blood samples were also collected at 0, 2, 4 and 6 hpt after treatment administration on day 5. Animals were humanly euthanized 24 h after the last dose administration using 18.2 mg/kg of pentobarbital sodium intravenously under tiletamine (4 mg/kg) and zolazepam (4 mg/kg) anesthesia. Samples of lung were collected at necropsy for HCQ quantification.

Determination of HCQ concentrations

Quantification of HCQ in plasma, blood and lung tissues was performed by a sensitive and selective validated high-performance liquid chromatography coupled with tandem mass spectrometry method (Quattro Premier XE LC-MS/MS, Waters, USA) as previously described ¹, with lower limits of quantification of respectively 0.015 µg/mL for plasma and 0.05 µg/mL for blood and lung tissue. Blood samples were centrifuged within 1-hour to collect plasma samples. Lung biopsies collected after euthanasia were thoroughly rinsed with cold 0.9% NaCl to remove blood contamination and blotted with filter paper. Then, each lung biopsy was weighed and homogenized with 1 ml of 0.9% NaCl using a Mixer mill MM200 (Retsch, Germany). Cellular debris was removed by centrifugation, and the supernatant was stored at -80°C.

HCQ was extracted by a simple protein precipitation method, using methanol for plasma and ice-cold

acetonitrile for blood and tissue homogenates. Briefly, 100 μ L of samples matrix was spiked with 10 μ L of internal standard working solution (HCQ-d5, Alsachim), then vortexed for 2 minutes followed by centrifugation for 10 minutes at 4°C. The supernatant was evaporated for blood and tissue homogenate samples. Dry residues or plasma supernatants were then transferred to 96-well plates and 5 μ L was injected. To assess the selectivity and specificity of the method and matrix effect, blank plasma, blood and tissues from control animals were processed and compared with that of HCQ and IS-spiked plasma, blood or tissue homogenate samples. Furthermore, each baseline sample (H0) of treated animals was processed in duplicate, including one spiked with HCQ prepared equivalent to quality control samples (QCs).

Concentrations in blood (μ g/mL), plasma (μ g/mL) and lung (μ g/g) were determined for each uninfected animal, and in plasma only for infected animals. Drug accumulation in lung was assessed by calculating a lung to blood and a lung to plasma concentration ratio as recently.

HCQ plasma trough concentrations determined within the context of routine therapeutic drug monitoring using the same method, 3 to 5 days after initiation of HCQ at 200 mg three times daily were provided for comparison.

Viruses and cells

For the *in vivo* studies, SARS-CoV-2 virus (hCoV-19/France/IDF0372/2020 strain) was isolated by the National Reference Center for Respiratory Viruses (Institut Pasteur, Paris, France) as described in Lescure et al.⁵. Virus stocks used *in vivo* were produced by two passages on VeroE6 cells in DMEM (Dulbecco's Modified Eagles Medium) without FBS, supplemented with 1% PS (penicillin at 10,000 U/ml and streptomycin at 10,000 μ g/mL) and 1 μ g/mL TPCK-trypsin at 37°C in a humidified CO₂ incubator and titrated on Vero E6 cells.

For the *in vitro* studies, the viral strain hCoV-19/France/IDF0571/2020 was provided by Dr. X. Lescure and Prof. Y. Yazdanpanah from the Bichat Hospital, Paris, France, where the isolate was obtained from another patient returning from Jichang (China) and passaged three times. For the virus used in the *in vivo* experiments, whole genome sequencing was performed as described in Lescure et al. with no modifications observed compared with the initial specimen⁵. For sequencing of the virus used *in vitro*,

viral RNA extraction was done using the QiAmp viral RNA Kit (Qiagen). The complete viral genome sequence was obtained using Illumina MiSeq sequencing technology. Sequences were deposited after assembly on the GISAID EpiCoV platform under accession numbers ID EPI_ISL_406596 for hCoV-19/France/IDF0372/2020 and EPI_ISL_411218 for hCoV-19/France/IDF0571/2020.

Viral replication kinetics and antiviral treatment in VeroE6 cells

VeroE6 cells were seeded 24 h in advance in multi-well 6 plates, washed twice with PBS and then infected with SARS-CoV-2 at the indicated MOIs. For HCQ treatment, the inoculum of infected VeroE6 was removed 1 hpi and cells were immediately treated with solutions in DMEM of HCQ. Supernatants were collected at 48 and 72 hpi and stored at -80°C for RNA extraction and viral quantification.

Viral quantification in VeroE6 cells

Viral stocks and collected samples were titrated by tissue culture infectious dose 50% (TCID₅₀/ml) in VeroE6 cells, using the Reed & Muench statistical method. Relative quantification of viral genome was performed by one-step real-time quantitative reverse transcriptase and polymerase chain reaction (RT-qPCR) from viral RNA extracted using QiAmp viral RNA Kit (Qiagen) in the case of supernatants/apical washings. Primer and probe sequences were selected from those designed by the School of Public Health/University of Hong Kong (Leo Poon, Daniel Chu and Malik Peiris) and synthesized by Eurogentec. Real-time one-step RT-qPCR was performed using the EXPRESS One-Step Superscript™ qRT-PCR Kit (Invitrogen, reference 1178101K) Thermal cycling was performed in a StepOnePlus™ Real-Time PCR System (Applied Biosystems) in MicroAmp™ Fast Optical 96-well reaction plates (Applied Biosystems, reference 4346907), as described in Pizzorno et al 2.

Viral infection and treatment in reconstituted human airway epithelia (HAE)

MucilAir™ HAE reconstituted from human primary cells obtained from nasal or bronchial biopsies were provided by Epithelix SARL (Geneva, Switzerland) and maintained in air-liquid interphase with specific culture medium in Costar Transwell inserts (Corning, NY, USA) according to the manufacturer's instructions. For infection experiments, apical poles were gently washed twice with warm OptiMEM medium (Gibco, ThermoFisher Scientific) and then infected directly with a 150 µl dilution of virus in OptiMEM medium, at a multiplicity of infection (MOI) of 0.1. For mock infection, the same procedure was performed using OptiMEM as inoculum. Samples collected from apical washes or

basolateral medium at different time-points were separated into 2 tubes: one for TCID50 viral titration and one RT-qPCR. HAE cells were harvested in RLT buffer (Qiagen) and total ARN was extracted using the RNeasy Mini Kit (Qiagen) for subsequent RT-qPCR and Nanostring assays. Treatments with HCQ were applied through basolateral poles. All treatments were initiated on day 0 (1h after viral infection) and continued once daily. Samples were collected at 48 hpi. Variations in transepithelial electrical resistance (Δ TEER) were measured using a dedicated volt-ohm meter (EVOM2, Epithelial Volt/Ohm Meter for TEER) and expressed as Ohm/cm².

Virus quantification in NHP samples

Upper respiratory (nasal and tracheal) and rectal specimens were collected with swabs (Universal transport medium, Copan, Italy or Viral Transport Medium, CDC, DSR-052-01). All specimens were stored between 2°C and 8°C until analysis with a plasmid standard concentration range containing an RdRp gene fragment including the RdRp-IP4 RT-PCR target sequence. The protocol describing the procedure for the detection of SARS-CoV-2 is available on the WHO website

https://www.who.int/docs/default-source/coronaviruse/real-time-rt-pcr-assays-for-the-detection-of-sars-cov-2-institut-pasteur-paris.pdf?sfvrsn=3662fcb6_2).

Plasma cytokine analysis

Cytokines were quantified in EDTA plasma using NHP ProcartaPlex immunoassay (ThermoFisher Scientific) for IFN- α , IL-1RA, IL-1 β , CCL-2/MCP-1, CCL-11/eotaxin, CXCL-11/ITAC, CXCL-13/BLC, granzyme B and PDGF-BB, using NHP Milliplex (Millipore) for CD40L, G-CSF, GM-CSF, IFN- γ , IL-2, IL-4, IL-5, IL-6, IL-8/CXCL-8, IL-10, IL-13, IL-15, IL-17A, CCL-3/MIP-1 α , CCL-4/MIP-1 β , TNF- α , VEGF and a Bioplex 200 analyzer (Bio-Rad) according to manufacturer's instructions.

Chest computed tomography and image analysis

Acquisition was done using a computed tomography (CT) system (Vereos-Ingenuity, Philips) in BSL-3 containment on anaesthetized animals placed in a supine position and monitored for heart rate, oxygen saturation and body temperature. A bolus of iodine contrast agent (Vizipaque 320 mg I/mL, GE Healthcare, 3mL/kg) was injected (Medrad CT Stellant® injector, Bayer) in the saphenous vein seconds prior to the initiation of CT acquisition. The CT detector collimation was 64 × 0.6 mm, the tube voltage was 120 kV and intensity of about 120mAs. Automatic dose optimization tools (Dose

Right, Z- DOM, 3D-DOM by Philips Healthcare) regulated the intensity. CT Images were reconstructed with a slice thickness of 1.25 mm and an interval of 0.25 mm.

Images were analyzed using INTELLISPACE PORTAL 8 software (Philips healthcare). All images had the same window level of -300 and window width of 1600. Lesions were defined as ground glass opacity, crazy-paving pattern, or consolidation or pleural thickening as previously described 3,4. Lesions and scoring were assessed independently in each lung lobe by two persons, and final results were made by consensus. Overall CT score includes lesion type (scored from 0 to 3) and lesion volume (scored from 0 to 4) summed for each lobe as detailed in Extended Data Fig. 3.

Statistical analysis

The following viral kinetic parameters were calculated in each experimental group as medians (min-max): viral load peak, area under the curve (AUC) of the log₁₀ viral load, time to first unquantifiable viral load. Each viral kinetic parameter was compared to untreated animals using Wilcoxon or Log-rank tests. To evaluate a potential effect of drug exposure on viral dynamics, we further evaluated the correlation of the viral kinetic parameters with the plasma concentrations of HCQ, taking the mean trough concentrations observed in each infected animal between 1 and up to day 15 post treatment as a marker for drug exposure during treatment period (Spearman test, without adjusting for tests multiplicity).

Methods references

1. Chhonker, Y. S., Sleightholm, R. L., Li, J., Oupicky, D. & Murry, D. J. Simultaneous quantitation of hydroxychloroquine and its metabolites in mouse blood and tissues using LC-ESI- MS/MS: An application for pharmacokinetic studies. *J Chromatogr B Analyt Technol Biomed Life Sci* **1072**, 320-327, doi:10.1016/j.jchromb.2017.11.026 (2018).
2. Pizzorno, *et al.* Characterization and treatment of SARS-CoV-2 in nasal and bronchial human airway epithelia. *bioRxiv*, 2020.2003.2031.017889, doi:10.1101/2020.03.31.017889 (2020).
3. Shi, H. *et al.* Radiological findings from 81 patients with COVID-19 pneumonia in

Wuhan, China: a descriptive study. *Lancet Infect Dis*, doi:10.1016/s1473-3099(20)30086-4 (2020).

4. Pan, F. *et al.* Time Course of Lung Changes On Chest CT During Recovery From 2019 Novel Coronavirus (COVID-19) Pneumonia. *Radiology*, 200370, doi:10.1148/radiol.2020200370 (2020).
5. Lescure, F. X. *et al.* Clinical and virological data of the first cases of COVID-19 in Europe: a case series. *Lancet Infect Dis*, doi:10.1016/s1473-3099(20)30200-0 (2020).

Declarations

Acknowledgements

Delache B, Burban E, Demilly J, Dhooge N, Langlois S, Le Calvez P, Potier M, Relouzat F, Robert JM and Dodan C contributed to animal studies. Fert B and Mayet C contributed to *in vivo* imaging studies. Pascal Q performed the necropsies. Morin J did the cytokines measurements and reagents preparation. Barthelemy K, Basso M, Doudka N, Giocanti M, contributed to HCQ concentration measurements. Lacarelle B and Guilhaumou R contributed to internal drug concentration data. Bertrand J contributed to pharmacokinetics analysis. Desjardins D contributed to the AZTH pharmacokinetic study. Aubenque C, Barendji M, Bossevot L, Dimant N, Dinh J, Gallouet AS, Leonec M, Mangeot I and Storck K contributed to sample processing. Albert M., Barbet M. and Donati F contributed to the production, titration and sequencing of the virus stocks used *in vivo* and to processing of samples for RT-PCR. Gallouet AS, Keyser, S, Marcos-Lopez E, Targat B and Vaslin B helped to experimental studies in the context of COVID-19 induced constraints. Ducancel F and Gorin Y contributed to logistics and safety management. We are very grateful for the help of Dr Sultan E from Sanofi for providing guidance in HCQ dose selection and discussion on PK/PD results and the review of the article.

We thank Sanofi for providing the hydroxychloroquine batch used in these experiments.

This study received financial support from REACTing, the National Research Agency (ANR - AM- CoV-Path) and the European Union's Horizon 2020 (H2020) research and innovation program (Fight- nCov - grant No 101003555). The virus stock was obtained through the EVAg platform

(<https://www.european-virus-archive.com/>) funded by H2020 (Grant No 653316). We thanks the Fondation Bettencourt Schueller and the Region Ile-de-France for the contribution to the implementation of imaging facilities. We thanks the Domaine d'Intérêt Majeur (DIM, Paris, France) "One Health" for its support. The Infectious Disease Models and Innovative Therapies research infrastructure (IDMIT) is supported by the "Programme Investissements d'Avenir" (PIA), managed by the ANR under reference ANR-11-INBS-0008.

Author contributions

BS: Performed RT-PCR viral quantification and analyzed the data. BA: Performed RT-PCR viral quantification and analyzed the data, CC: Coordinated of imaging facility. CV: Contributed to data analysis, statistical analyses, and figures and article writing. DBN: Contributed to the animal work and cytokine measurement, analysed the data, coordinated IDMIT core activities. DLX: Contribute to study design and PK/PD analysis and article writing. EN: Developed the qPCR assay and analyzed the data. GJ: Contributed to data analysis, contributed to PK/PD study and article writing. HTFR: Coordinated animal core facility, contributed to study design and data analysis. HB: Contributed to study design, data analysis and article writing. KN: Performed CT acquisitions and acquisition parameters design, contributed to data analysis. RLG: Conceived the project, designed the study, coordinated the work, analyzed the data and wrote the article. LJ: contributed to clinical follow up of animals, data analysis and article writing. LB: Coordinated the in vitro evaluation of HCQ (Vero E6, HAE), analyzed the data and contributed to writing the article. MP: Contributed to project conception and design of the study, contributed to animal drug, contributed to coordination of the experiments and data analysis, and article writing. MR: Contributed to the design of the study, animal work and data analysis and contributed to article writing. NT: Performed CT acquisitions / CT quantification & quantification design / CT figures and article writing. PA: Performed in vitro evaluation of HCQ (Vero E6, HAE), contributed to data analysis and manuscript preparation. RCM: Designed the in vitro evaluation of HCQ (Vero E6, HAE), supervised and coordinated the work, analyzed the data and contributed to writing the article. SC: Supervised and coordinated the HCQ PK analysis, contributed to article writing. TF: contributed to in vitro antivirals evaluation. TO: Performed in vitro evaluation of HCQ (Vero E6,

HAE), contributed to data analysis and manuscript preparation.VDWS: Conceived the project, designed the study, provided the viral challenge stock, coordinated the viral load quantification, analyzed the data and article writing.

Competing interest declaration

The authors declare that they have no conflict of interest.

Additional information:

***Corresponding author:** Roger Le Grand, CEA, UMR1184, IDMIT Department, 18 route du Panorama, 92265, Fontenay-aux-Roses, France ; Tel +33 1 46 54 87 57 ; FAX : +33 1 46 54 77 26 ; [roger.le- grand@cea.fr](mailto:roger.le-grand@cea.fr)

Pauline Maisonnasse, Jérémie Guedj, Vanessa Contreras, Sylvie Behillil, Caroline Solas and Romain Marlin have equally contributed to the work

Extended data figures are presented in a separate file

References

1. Li, Q. *et al.* Early Transmission Dynamics in Wuhan, China, of Novel Coronavirus-Infected Pneumonia. *N Engl J Med* **382**, 1199-1207, doi:10.1056/NEJMoa2001316 (2020).
2. He, X. *et al.* Temporal dynamics in viral shedding and transmissibility of COVID-19. *Nature medicine*, doi:10.1038/s41591-020-0869-5 (2020).
3. Huang, C. *et al.* Clinical features of patients infected with 2019 novel coronavirus in Wuhan, China. *Lancet (London, England)* **395**, 497-506, doi:10.1016/s0140-6736(20)30183-5 (2020).
4. Chen, *et al.* Clinical and immunological features of severe and moderate coronavirus disease 2019. *J Clin Invest*, doi:10.1172/jci137244 (2020).
5. Liu, Y. *et al.* Viral dynamics in mild and severe cases of COVID-19. *Lancet Infect Dis*, doi:10.1016/s1473-3099(20)30232-2 (2020).
6. Touret, F. & de Lamballerie, X. Of chloroquine and COVID-19. *Antiviral Res* **177**,

- 104762, doi:10.1016/j.antiviral.2020.104762 (2020).
7. Touret, F. *et al.* *In vitro* screening of a FDA approved chemical library reveals potential inhibitors of SARS-CoV-2 replication. *bioRxiv*, 2020.2004.2003.023846, doi:10.1101/2020.04.03.023846 (2020).
 8. Wang, M. *et al.* Remdesivir and chloroquine effectively inhibit the recently emerged novel coronavirus (2019-nCoV) in vitro. *Cell Res* **30**, 269-271, doi:10.1038/s41422-020-0282-0 (2020).
 9. Liu, *et al.* Hydroxychloroquine, a less toxic derivative of chloroquine, is effective in inhibiting SARS-CoV-2 infection in vitro. *Cell Discov* **6**, 16, doi:10.1038/s41421-020-0156-0 (2020).
 10. Ponticelli, C. & Moroni, G. Hydroxychloroquine in systemic lupus erythematosus (SLE). *Expert Opin Drug Saf* **16**, 411-419, doi:10.1080/14740338.2017.1269168 (2017).
 11. Savarino, A., Di Trani, L., Donatelli, I., Cauda, R. & Cassone, A. New insights into the antiviral effects of *Lancet Infect Dis* **6**, 67-69, doi:10.1016/s1473-3099(06)70361-9 (2006).
 12. Rainsford, D., Parke, A. L., Clifford-Rashotte, M. & Kean, W. F. Therapy and pharmacological properties of hydroxychloroquine and chloroquine in treatment of systemic lupus erythematosus, rheumatoid arthritis and related diseases. *Inflammopharmacology* **23**, 231- 269, doi:10.1007/s10787-015-0239-y (2015).
 13. Schrezenmeier, & Dorner, T. Mechanisms of action of hydroxychloroquine and chloroquine: implications for rheumatology. *Nat Rev Rheumatol* **16**, 155-166, doi:10.1038/s41584-020- 0372-x (2020).
 14. Monzavi, S. M. *et al.* Efficacy analysis of hydroxychloroquine therapy in systemic lupus erythematosus: a study on disease activity and immunological biomarkers.

- Inflammopharmacology* **26**, 1175-1182, doi:10.1007/s10787-018-0512-y (2018).
15. Fanouriakis, A. *et al.* 2019 Update of the Joint European League Against Rheumatism and European Renal Association-European Dialysis and Transplant Association (EULAR/ERA-EDTA) recommendations for the management of lupus nephritis. *Ann Rheum Dis*, doi:10.1136/annrheumdis-2020-216924 (2020).
 16. Zhang, B. *et al.* Macrolide derivatives reduce proinflammatory macrophage activation and macrophage-mediated neurotoxicity. *CNS Neurosci Ther* **25**, 591-600, doi:10.1111/cns.13092 (2019).
 17. Gautret, P. *et al.* Clinical and microbiological effect of a combination of hydroxychloroquine and azithromycin in 80 COVID-19 patients with at least a six-day follow up: A pilot observational study. *Travel Med Infect Dis*, 101663, doi:10.1016/j.tmaid.2020.101663 (2020).
 18. Magagnoli, J. *et al.* Outcomes of hydroxychloroquine usage in United States veterans hospitalized with Covid-19. *medRxiv*, 2004.2016.20065920, doi:10.1101/2020.04.16.20065920 (2020).
 19. Rockx, B. *et al.* Comparative pathogenesis of COVID-19, MERS, and SARS in a nonhuman primate model. *Science*, eabb7314, doi:10.1126/science.abb7314 (2020).
 20. Williamson, *et al.* Clinical benefit of remdesivir in rhesus macaques infected with SARS-CoV-2. *bioRxiv*, 2020.2004.2015.043166, doi:10.1101/2020.04.15.043166 (2020).
 21. Yao, X. *et al.* In Vitro Antiviral Activity and Projection of Optimized Dosing Design of Hydroxychloroquine for the Treatment of Severe Acute Respiratory Syndrome Coronavirus 2 (SARS-CoV-2). *Clin Infect Dis*, doi:10.1093/cid/ciaa237 (2020).
 22. Nicolas de Lamballerie, C. *et al.* Characterization of cellular transcriptomic signatures induced by different respiratory viruses in human reconstituted airway epithelia. *Sci*

- Rep* **9**, 11493, doi:10.1038/s41598-019-48013-7 (2019).
23. Pizzorno, *et al.* Characterization and treatment of SARS-CoV-2 in nasal and bronchial human airway epithelia. *bioRxiv*, 2020.2003.2031.017889, doi:10.1101/2020.03.31.017889 (2020).
24. Pan, F. *et al.* Time Course of Lung Changes On Chest CT During Recovery From 2019 Novel Coronavirus (COVID-19) Pneumonia. *Radiology*, 200370, doi:10.1148/radiol.2020200370 (2020).
25. Shi, *et al.* Radiological findings from 81 patients with COVID-19 pneumonia in Wuhan, China: a descriptive study. *Lancet Infect Dis*, doi:10.1016/s1473-3099(20)30086-4 (2020).
26. Chen, *et al.* Epidemiological and clinical characteristics of 99 cases of 2019 novel coronavirus pneumonia in Wuhan, China: a descriptive study. *Lancet (London, England)* **395**, 507-513, doi:10.1016/s0140-6736(20)30211-7 (2020).
27. Roques, P. *et al.* Paradoxical Effect of Chloroquine Treatment in Enhancing Chikungunya Virus Infection. *Viruses* **10**, doi:10.3390/v10050268 (2018).

Figures

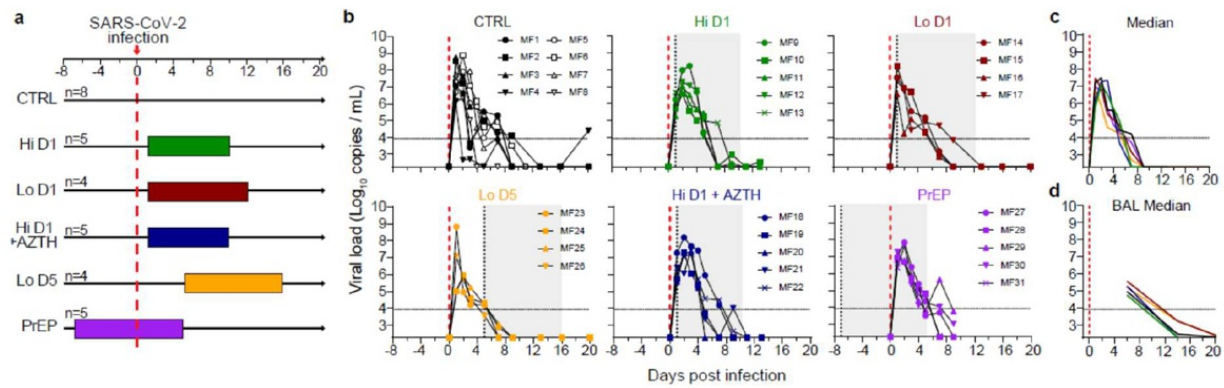


Figure 1

Study design and viral loads in the respiratory tract of SARS-CoV-2 infected cynomolgus macaques treated with hydroxychloroquine and azithromycin. a, Study design. Each group of cynomolgus macaques is represented by one line. The red dotted line indicates infection with 106 pfu of SARS-CoV-2 by the combined intra-nasal and intratracheal routes. Colored areas indicate hydroxychloroquine (HCQ) treatment periods. Each group received either a high (Hi) dose regimen of HCQ, or a low (Lo) dose regimen. The treatment started 1 day (D1) or 5 days (D5) after exposure, or 7 days before viral challenge for the pre-exposure prophylaxis (PrEP) group. In combination with HCQ, one group received azithromycin (AZTH). The control group (CTRL) received vehicle (water) as placebo. Viral loads by PCR in throat swabs (b, c) and broncho-alveolar lavages (BAL) (d). The limit of detection was estimated to 2.3 log₁₀ copies of SARS-CoV-2 RNA per mL and the limit of quantification was estimated to 3.9 log₁₀ copies per mL (dotted horizontal line). b, Shaded zones indicate treatment periods. c, d, Data are represented as medians of each group.

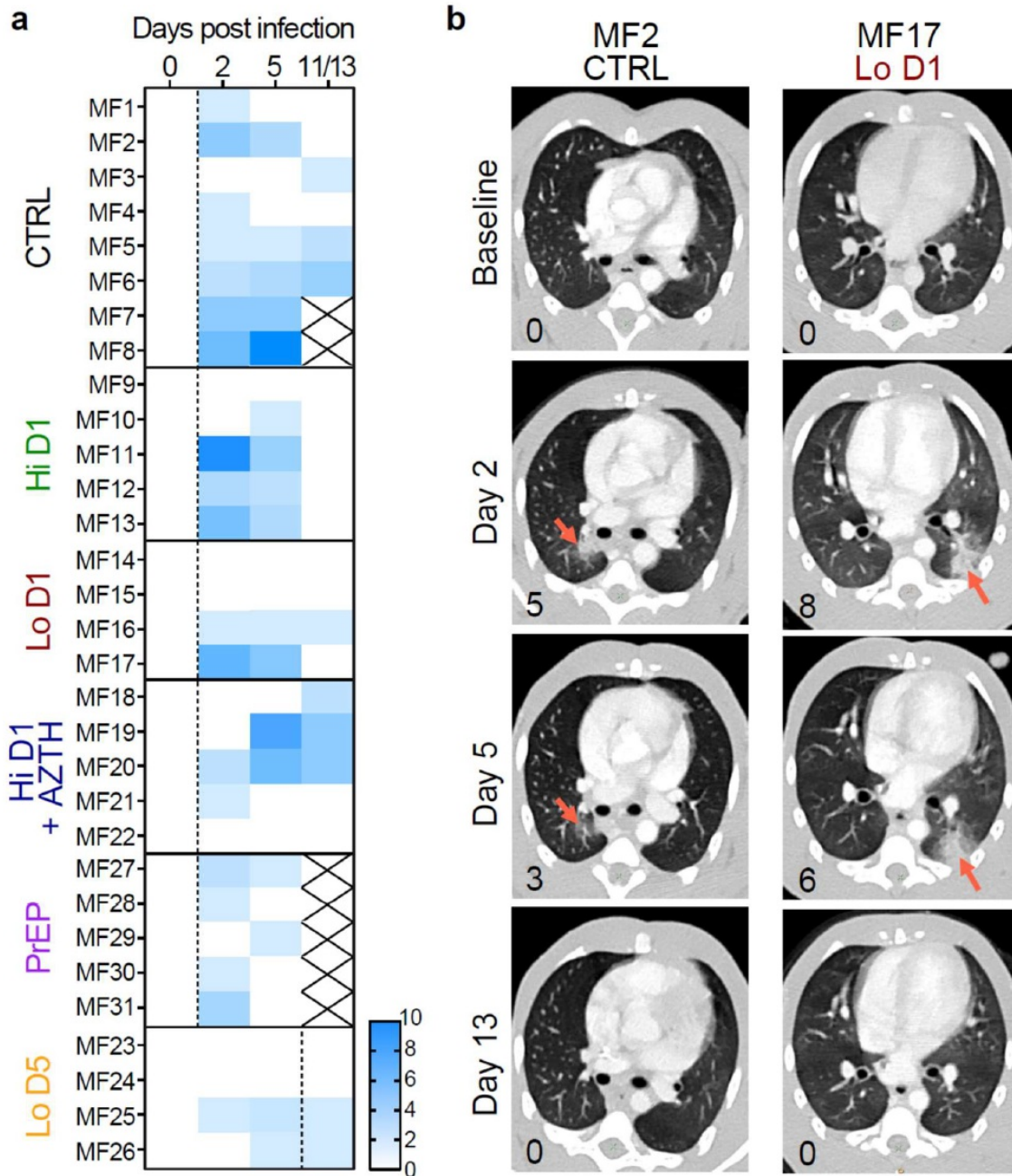


Figure 2

Time course of lung lesions by CT in SARS-CoV-2 infected cynomolgus macaques treated with hydroxychloroquine. Lung lesions were assessed by chest CT before infection with SARS-CoV-2 and at days 2, 5 and 11 or 13 pi. a, Heatmap of the overall CT score. Scores include lesion types (ground-glass opacity, crazy-paving pattern, consolidation or pleural thickening (scored from 0 to 3) and lesions volume (scored from 0 to 4) summed for each lobe. Scores are consensus values from two independent evaluators. Dotted lines indicate

treatment initiation. b, Illustration of lung lesions in two animals at baseline, day 2, day 5 and day 13 pi. Red arrows indicate typical lesions. Numbers at the bottom left of each image represent the CT score associated to this animal and time-point.

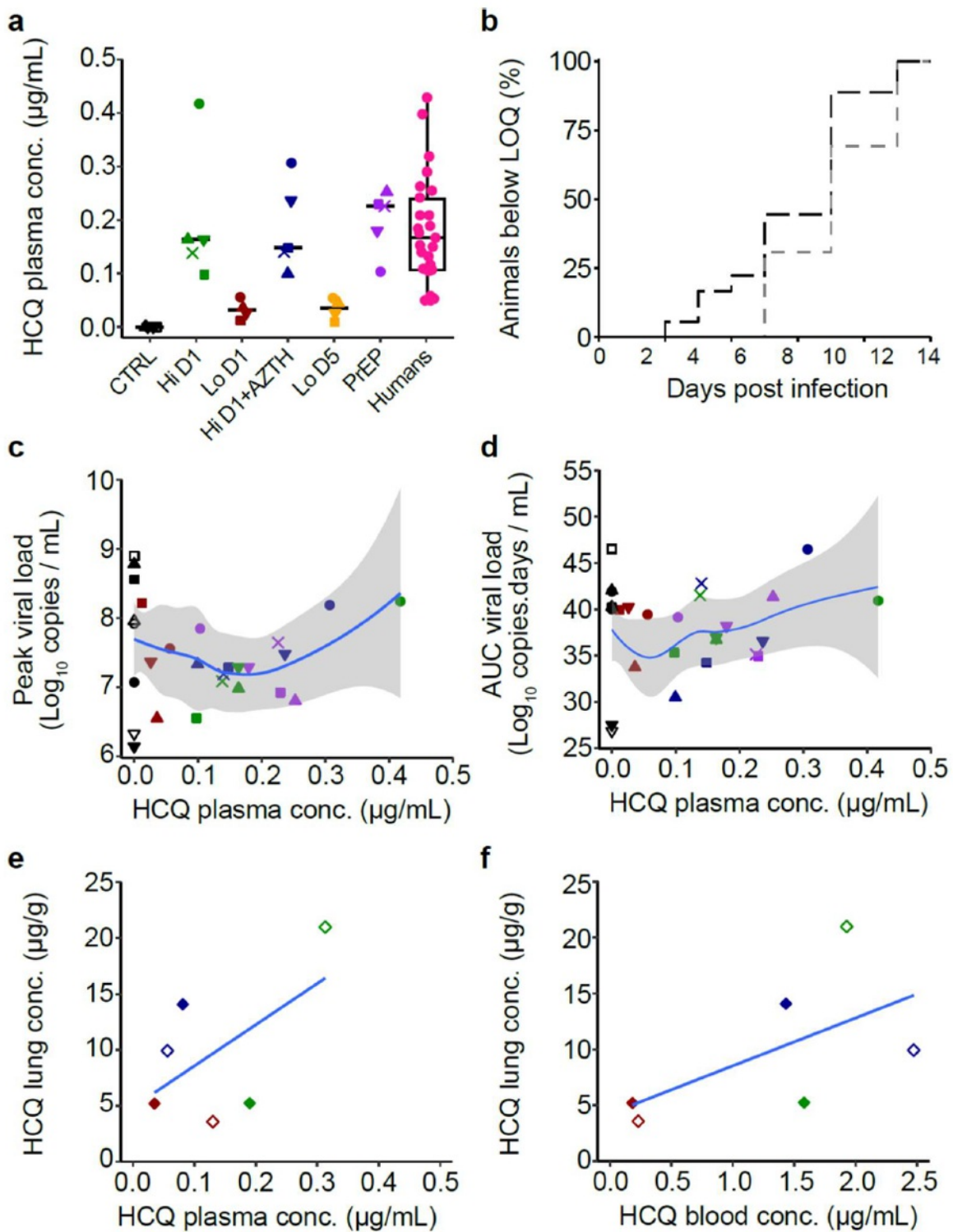


Figure 3

Pharmacokinetics and viral kinetics parameters in cynomolgus macaques a, Individual mean

plasma trough concentration of HCQ in macaques during treatment and internal patients data (n=25). b, Time to the first measurement below the limit of quantification in macaques having mean plasma trough concentration <0.1 µg/mL (black) and >0.1 µg/mL (grey). c, Peak viral load according to mean HCQ plasma trough concentration. d, Area under the curve (AUC) or viral kinetic curves between 1 and 9 days pi. e, Correlation between HCQ lung and plasma concentrations. f, Correlation between HCQ lung and blood concentrations.

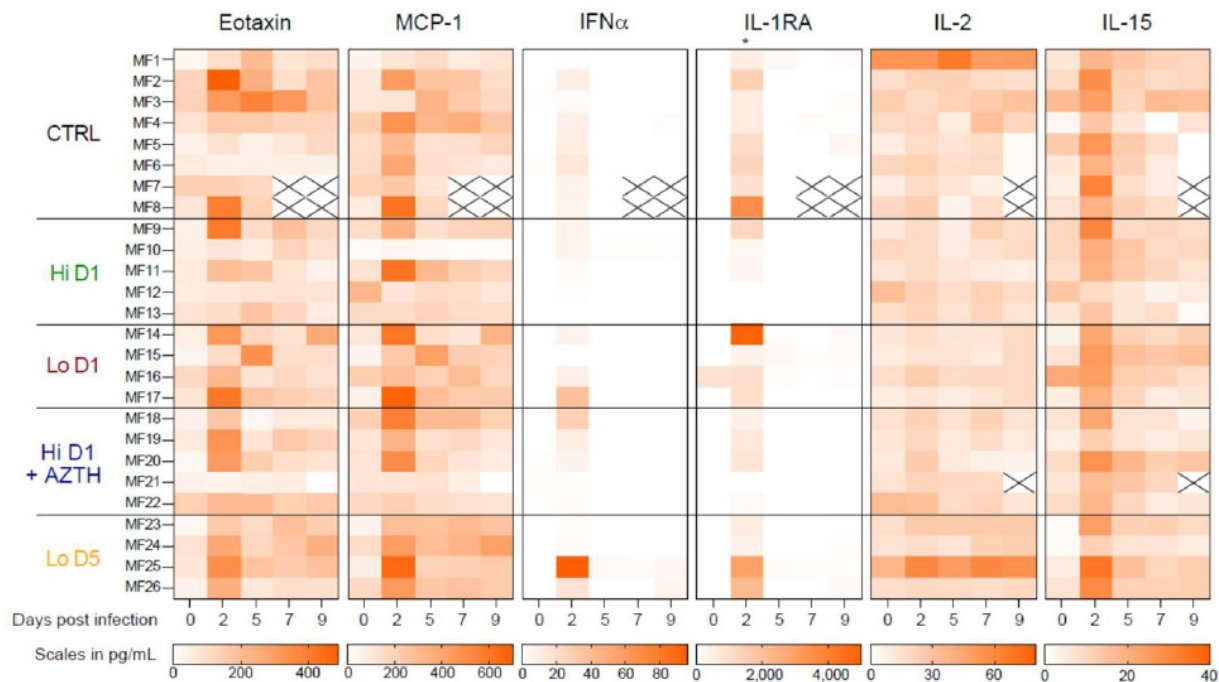


Figure 4

Cytokines and chemokines in the plasma of SARS-CoV-2 exposed cynomolgus macaques treated with hydroxychloroquine (a) Heatmap of plasma concentrations of eotaxin/CCL11, MCP-1/CCL2, IFN- α , IL-1RA, IL-2 and IL-15 at days 0, 2, 5, 7 and 9 pi. Scales are in pg/mL. Asterisks (*) represent a significant difference at one time- point between the CTRL group and the Hi D1 and/or Hi D1 + AZTH groups. Statistical significance was determined using a two-sided Mann-Whitney U-test.

Supplementary Files

This is a list of supplementary files associated with this preprint. Click to download.

ExtendedData.pdf

